Title: Electronic blood vessel

Authors: Shiyu Cheng[1,2,4†], Chen Hang[1,2†], Li Ding[1,2,3†], Liujun Jia[3], Lixue Tang[2], Lei Mou[1,2], Jie Qi[1,2], Ruihua Dong[1,2], Wenfu Zheng[2], Yan Zhang[3]*, Xingyu Jiang[1,2]*

Affiliations:

[1]Department of Biomedical Engineering and Shenzhen Bay Laboratory, Southern University of Science and Technology, Shenzhen, Guangdong 518055, China.

[2]National Center for NanoScience and Technology, University of Chinese Academy of Sciences, Beijing 100190, China.

[3]State Key Laboratory of Cardiovascular Disease, Fuwai Hospital, National Center for Cardiovascular Diseases, Chinese Academy of Medical Sciences and Peking Union Medical College, Beijing 100037, China.

[4]Current address: Institute of Bioengineering, School of Engineering, Ecole Polytechnique Federale de Lausanne, Lausanne 1015, Switzerland.

*To whom correspondence should be addressed: jiang@sustech.edu.cn; waikezhangyan@126.com

†These authors contributed equally to this work.

Abstract

Advances in bioelectronics have great potential to address unsolvable biomedical problems in the cardiovascular system. By using poly(L-lactide-co-ε-caprolactone) (PLC) that encapsulates the liquid metal to make flexible and bio-degradable electrical circuitry, we develop an electronic blood vessel that can integrate flexible electronics with three layers of blood vessel cells, to mimic and go beyond the natural blood vessel. It can improve the endothelization process through electrical stimulation and can enable controlled gene delivery into specific part of the blood vessel via electroporation. The electronic blood vessel has excellent biocompatibility in the vascular system and shows great patency three months post-implantation in a rabbit model. The electronic blood vessel would be an ideal platform to enable diagnostics and treatments in the cardiovascular system and can greatly empower personalized medicine by creating a direct link of vascular tissue-machine interface.

Introduction

Cardiovascular diseases remain the number one cause of mortality worldwide[1]. In treating cardiovascular diseases via coronary artery bypass grafting (CABG) surgery, none existing small diameter (<6 mm) tissue engineered blood vessel (TEBV) has met clinical demands[2]. To fabricate the TEBV, a range of approaches, such as decellularized matrix[3–7], self-assembly cell sheets[8–11], bioactive and biomimetic materials[12–14], were developed and clinically investigated in recent years. However, most of these methods only serve as scaffolds to provide mechanical support and mainly rely on the remodeling process by the host tissue and present significant limitations in helping the regeneration of neo blood vessel. Thus far, none of them have achieved satisfactory clinical results. Specifically, a complex interplay between the blood flow and the TEBV can often cause inflammatory responses, resulting in thrombosis, neointimal hyperplasia or smooth muscle cell accumulation nearby the scaffold[2,15], in different pathological stages. To address these issues, next-generation TEBV should not only function as scaffolds to provide the mechanical support and facilitate host cell recruitments, but also have the capability to actively respond to and couple with the native remodeling process in order to provide adaptive treatments after implantation.

Combining living tissues with flexible electronics[16,17] could endow the conventional TEBV more functionalities and capabilities to overcome existing biomedical problems, such as precision diagnostics, by *in situ* sensing the blood flow and temperature, and treatments by therapeutic drug or gene delivery[18,19]. In previous

works, we have developed many approaches to fabricate structures that mimic natural blood vessel with multiple types of blood vessel cells in different layers, including stress-induced self-rolling membrane[13,20–22] and layer by layer technique[23]. Recently, we have developed a printable metal-polymer conductor (MPC) which exhibited excellent compatibility and high stretchability[24,25]. Here, we develop an electronic blood vessel that integrates flexible electrodes into the bio-degradable scaffold by combining the liquid metal with poly(L-lactide-co-ε-caprolactone) (PLC) into a metal-polymer conductor. We evaluated the efficacy and biosafety of the electronic blood vessel in the vascular system through a three-month *in vivo* study by using a rabbit carotid artery replacement model and confirmed its patency by using ultrasound imaging and arteriography. As a proof of principle, we used the electronic blood vessel to carry out *in vitro* electrical stimulation and electroporation. By electrical stimulation, the electronic blood vessel can effectively promote cell proliferation and migration in a wound healing model. It can also *in situ* deliver the GFP DNA plasmid into three kinds of blood vessel cells via electroporation. Our results pave the way to integrating flexible, degradable bio-electronics into the vascular system, which can serve as a platform to carry out further treatments, such as gene therapies, electrical stimulation, electronically controlled drug releases.

Results

Fabrication of the electronic blood vessel.

We fabricated the electronic blood vessel (**Fig. 1a**) by rolling up a PLC based metal-polymer conductor (MPC-PLC) membrane (**Fig. 1b**) with the assistance of a polytetrafluoroethylene (PTFE) mandrel. The MPC circuit was well distributed in the three dimensional (3D) multilayered tubular structure. The inner diameter of the electronic blood vessel was about 2 mm. The MPC-PLC membrane is flexible, conductive, and degradable (**Fig. 1b-d**). The conductivity of the MPC circuit is about $8*10^3$ S cm^{-1} and the ΔR/R of the circuit remained constant after around 1000 cycles of bending and rubbing (**Fig. 1c**). The PLC is projected to be entirely degraded around 1~2 years by the manufacturer. The MPC-PLC membrane underwent a mass loss of around 10% during 8-week incubation in the phosphate-buffered saline (37 ºC) (**Fig. 1d**). To fabricate the MPC-PLC membrane, we screen-printed the conductive ink on the polyethylene terephthalate (PET) membrane (**Fig. 1e**). The electrode design was optimized for electroporation and electrical stimulation (**Supplementary Fig. 1**). We prepared the liquid metal conductive ink by sonicating the mixture of Gallium-Indium alloy (EGAIn, ≥99.99%, Sigma, US) and the volatile solvent (1-decanol, Macklin, Shanghai) (**Fig. 1f, h**). The liquid metal particles (LMPs) exhibit a core-shell structure, where the core is the Ga-In alloy and the shell is the Ga-In Oxide (**Fig. 1g**). The diameter of the LMPs is around 2 μm (**Fig. 1j**). We embedded the LMPs-based circuit with the PLC solution (5 wt % in CH_2Cl_2) and peeled the MPC-PLC membrane off the PET substrate after evaporation of the solvent in a chemical hood

(**Fig. 1e**). The thickness of the MPC-PLC membrane is about 50 μm and it is tunable by changing the volume of the PLC solution. The LMPs could be broken during the process of peeling and release the Ga-In alloy to make the circuit conductive[25]. We confirmed the structure of the conductive circuit via corrosion of the Ga-In alloy by adding excessive hydrochloric acid (HCl, Beijing Chemical Works, China). The LMPs were evenly distributed in the cellular PLC host (**Fig. 1k, l**). The liquid metal could form a coherent conductive pathway in the polymeric host. We tested the mechanical properties of the electronic blood vessel for the *in vivo* study (**Fig. 1m-r**).

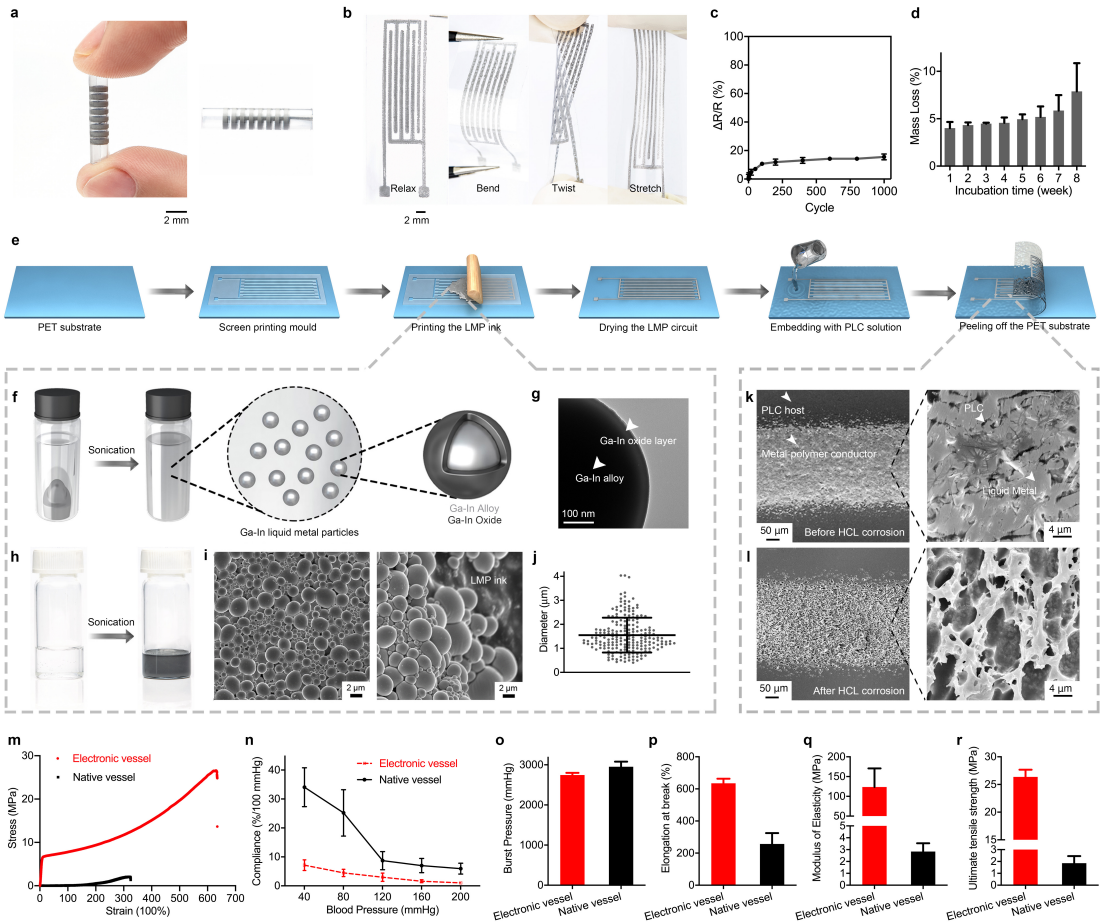

Fig. 1. Fabrication and characterization of the electronic blood vessel. a,

107 Snapshots of the electronic blood vessel. Scale bar, 4 mm. **b**, Snapshots of the MPC-
108 PLC membrane. Scale bar, 1 mm. **c**, ΔR/R changes with a bend of 180° for 1000
109 cycles (n=3). **d**, Mass loss of the MPC-PLC membrane during 8-week incubation
110 (n=3 for each time point). **e**, Schematic of fabrication of the MPC-PLC membrane. **f**,
111 Schematic of fabrication of LMPs. **g**, TEM image of the Ga-In particle. **h**,
112 Photographs of mixture of the Ga-In alloy and the solvent, and the LMP ink after
113 sonication. **i**, Representative SEM images of LMPs. Scale bar, 2 μm. **j**, Diameter
114 distribution of LMPs (n =200). **k**, SEM images of the MPC-PLC circuit. White
115 arrowheads indicate the PLC host and MPC-PLC membrane. Scale bar, 50 μm. Right
116 is the Zoom-in view. White arrowheads indicate the PLC and LMP ink. LMPs were
117 embedded by the PLC as the host polymer. Scale bar, 4 μm. **l**, SEM images of the
118 MPC-PLC circuit after corrosion by excessive hydrochloric acid. Scale bar, 50 μm.
119 Right is the Zoom-in view. LMPs were fully removed by corrosion. The porous
120 structure only consisted of the PLC. Scale bar, 4 μm. **m-r**, Mechanical properties of
121 the electronic blood vessel. **m**, Stress-strain curve. **n**, Compliance test. **o**, Burst
122 pressure test. **p**, Elongation at break. **q**, Modulus of elasticity. **r**, Ultimate tensile
123 strength. Electronic blood vessel (n= 5) and native carotid artery (n= 3) were used in
124 each test. All data are expressed as mean ± SD.
125
126 ***In vitro* characterization of the electronic blood vessel.**
127 To evaluate biocompatibility of the electronic blood vessel, we used the microfluidic
128 technology to realize accurate 3D pattern of three kinds of blood vessel cells in a

natural blood vessel mimicking fashion. By employing a multichannel microfluidic chip, we delivered human umbilical vein endothelial cells (HUVECs, blue), human aortic smooth muscle cells (SMCs, green), human aortic fibroblasts (HAFs, red) sequentially on the MPC-PLC membrane (**Fig. 2a-e**). We designed the width of each channel to match the circumference of each layer of the tube based on thickness of the MPC-PLC membrane and the diameter of the tube (**Fig. 2b**). To distinguish different cell types, we stained the HUVECs, SMCs, HAFs with different fluorescent dyes (HUVECs: Cell Tracker violet; SMCs: Cell Tracker green; HAFs: Cell Tracker deep red) before seeding them into the microfluidic chip. After 1 d incubation in culture medium (Dulbecco's modified eagle medium, DMEM, 10% FBS, 37 ^{o}C, 5% CO_2), cells attached on the MPC-PLC membrane (**Fig. 2d, h**). We peeled the microfluidic chip off the cell-laden MPC-PLC membrane and rolled it up with a PTFE mandrel, forming a 3D multi-layered tubular structure (**Fig. 2e-g**) with HUVECs, SMCs, and HAFs evenly distributed in inner layer, middle layer, and outer layers, respectively (**Fig. 2i, j**). This structure well mimics the structure of the natural blood vessel. We used a biomedical fibrin glue to facilitate the combination of different layers[18]. We incubated the cell-laden electronic blood vessel for 14 d and stained the cells with the Calcein AM green. The evenly distributed green color on the MPC-PLC membrane indicated that the cells exhibited high viability after a 14 d culture (**Fig. 2k**).

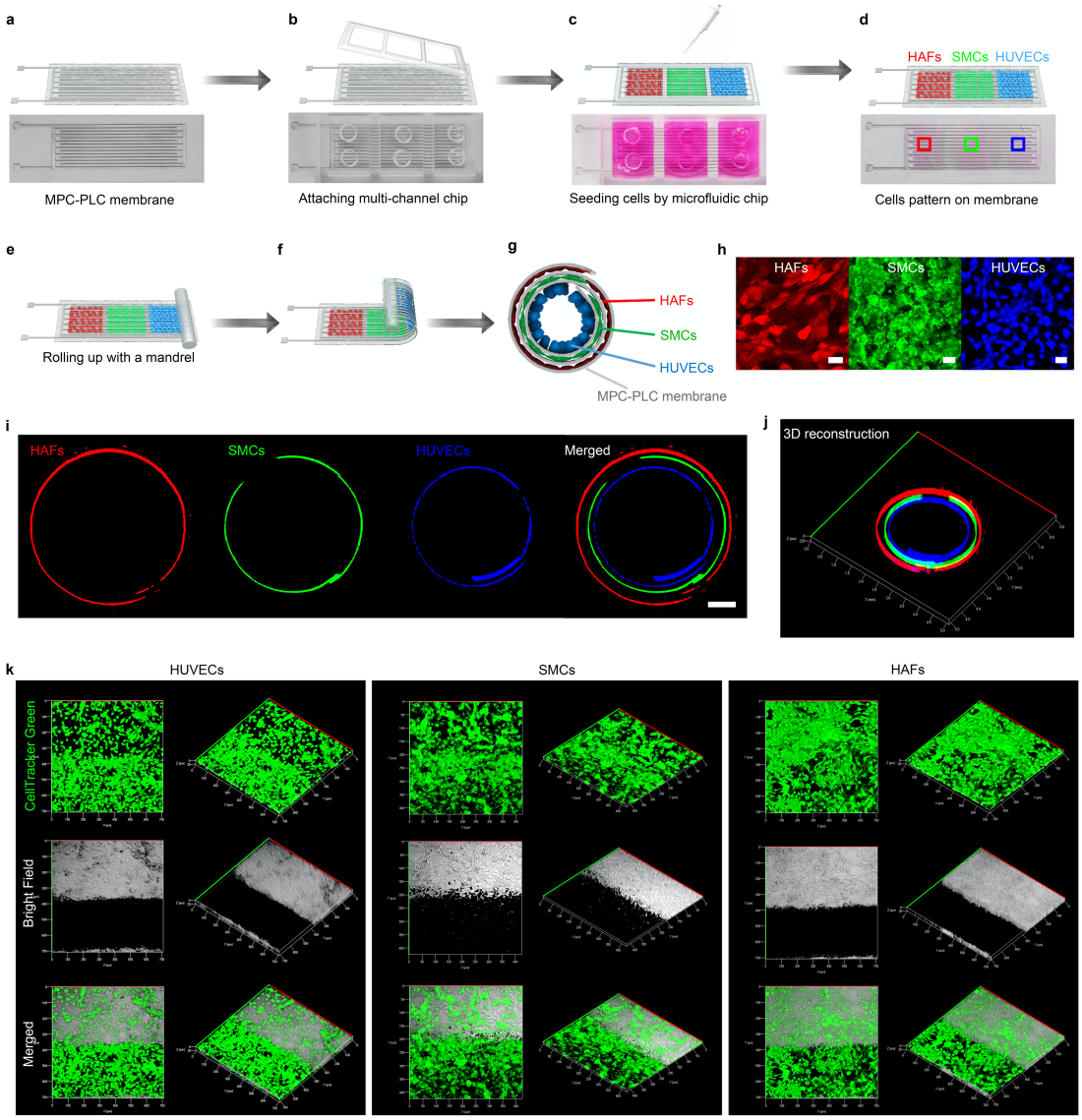

Fig. 2. *In vitro* biocompatibility of the electronic blood vessel. a, The MPC-PLC membrane. **b**, Attaching a multichannel microfluidic chip onto the MPC-PLC membrane. **c, d**, Patterning three kinds of blood vessel cells (blue: HUVECs, green: SMCs, red: HAFs) onto the MPC-PLC membrane by using PDMS microfluidic chip. **e, f**, Rolling the cell-laden membrane into a multi-layered tubular structure with a PTFE mandrel. **g**, Cross-sectional view of natural blood vessel mimicking structure with different cells distributed in different layers. **h**, Fluorescent images of cells on the MPC-PLC membrane, in corresponding to (**d**). Stained by CellTracker violet,

158 green, deep red, respectively. Scale bar, 20 μm. **i,** Three kinds of blood vessel cells
159 distributed in different layers of the electronic blood vessel. Scale bar, 500 μm. **j**, 3D
160 construction of (**i**). **k**, Cell viability after 2-week incubation in the electronic blood
161 vessel. Stained by CellTracker green. The right column is the 3D reconstruction of the
162 left column in each image. The black area represents the MPC circuit and the
163 transparent area represents the PLC in bright-field images.
164

165 ***In vitro* electrical stimulation promotes HUVEC proliferation and migration**

166 To prove the functionality of the electronic blood vessel, we carried out *in vitro*
167 electrical stimulation to improve proliferation and migration of HUVECs as a proof of
168 concept. Direct current (DC) electric field has been proved to effectively increase the
169 angiogenesis *in vitro* and *in vivo*[26]. We patterned HUVECs on the MPC-PLC
170 membrane (DMEM, 10% FBS, 37 °C, 5% CO_2) by using a multi-chamber PDMS
171 chip. The initial number of cells in each chamber was the same (3×10^4). After 12 h
172 incubation, we applied different DC voltages to yield different electrical field
173 strength: 25, 50, 75 100, 200, and 400 mV mm^{-1}, respectively (**Fig. 3a, b**). After 2 d
174 incubation and electrical stimulation, we randomly selected 6 different domains on
175 each sample and analyzed by using a laser scanning confocal microscopy (LSCM,
176 LSM 710, Zeiss, Germany). We stained nuclei (blue) with Hoechst 33342 (Invitrogen,
177 USA) and stained the living and dead cells with Calcein-AM (green) and PI (red),
178 respectively. The green cells occupied the whole domain, indicating that electrical
179 stimulation did not hurt proliferation of HUVECs (**Supplementary Fig. 2a**). We

180 counted the number of nuclei by using ImageJ. The cell number under 50 mV mm^{-1}

181 was highest (**Fig. 3d**), about 2.4 times that of the control (**Fig. 3e**). We used the CCK-

182 8 kit to confirm this conclusion (**Fig. 3f**). We speculated that the DC electric field had

183 selectively regulated production of certain growth factors and cytokines important for

184 angiogenesis.

185 We used a wound healing model to explore the migration of HUVECs under

186 different DC electric field strengths. We made a scratch on a PDMS substrate by using

187 a 10 μl tip. After application of an electric field of 50 mV mm^{-1}, HUVECs migrated

188 750 μm and the wound completely healed after 24 h (**Fig. 3g, f**). Different strengths

189 had enhanced migration differently compared to the control group without electrical

190 stimulation (**Supplementary Fig. 2b**). The *in vitro* DC electrical stimulation thus

191 proved to have effectively promoted the proliferation and migration of HUVECs.

192

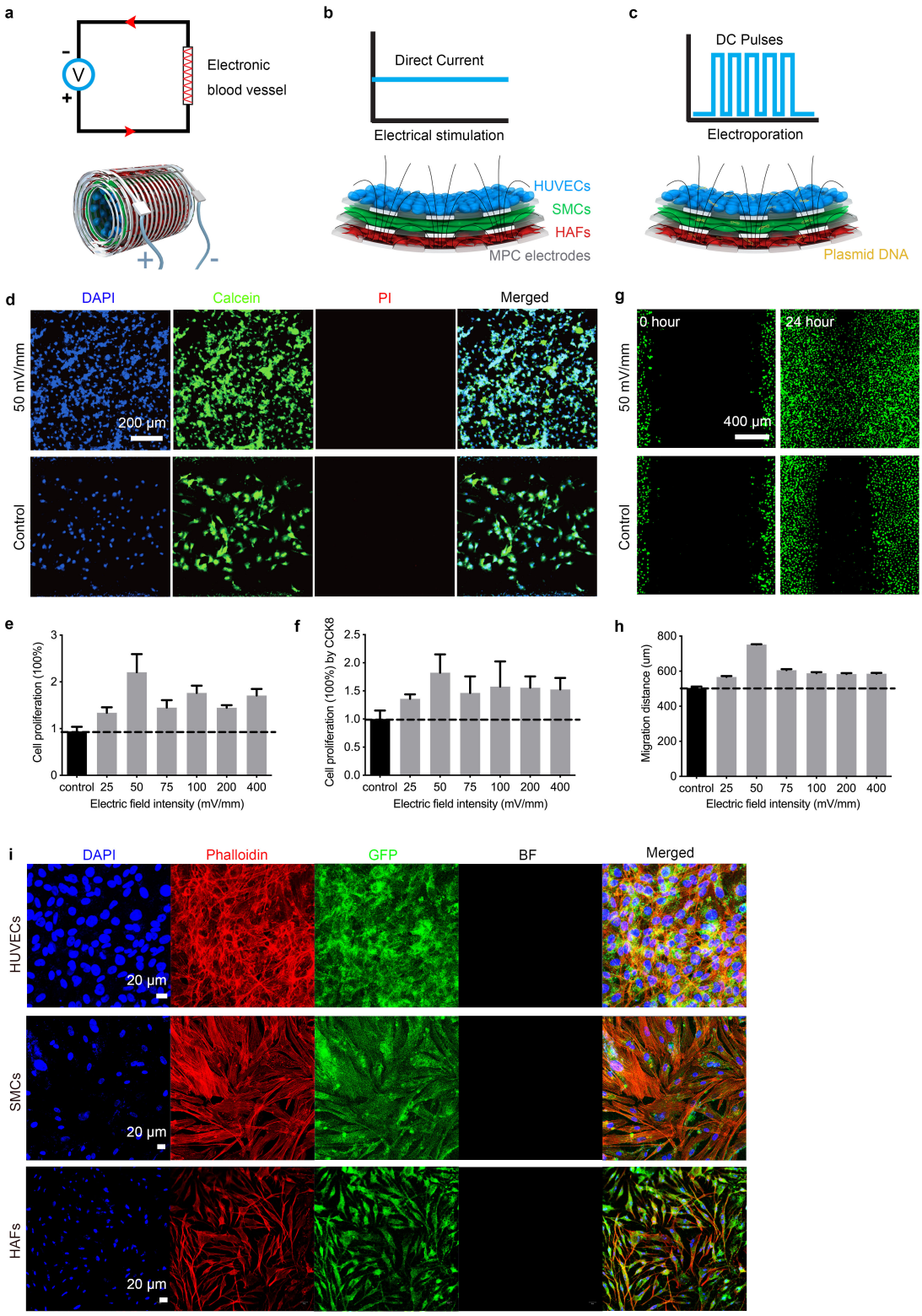

Fig. 3. *In vitro* electrical stimulation and electroporation. a-c, The electronic blood vessel was connected to electrochemical station to generate a direct current voltage (b) or an electroporator to generate electrical pulses (c). **d**, Confocal fluorescent

197 images of HUVECs after 2 d incubation and stimulation at a DC electric field of 50
198 mV mm^{-1}. Blue, DAPI; green, Calcein AM; red, PI. **e**, The proliferation of HUVECs
199 under different DC electrical field, setting the control (without electric field) as 100%.
200 (n=4). **f**, The proliferation of HUVECs under different DC electrical field tested with
201 the CCK-8 kit. (n=4). **g**, Confocal fluorescent images of HUVECs at a DC electrical
202 field of 50 mV mm^{-1} in a wound healing model. Scale bar, 400 μm. A 10 μl tip was
203 used to scratch a line for HUVECs migration. **h**, The migration of HUVECs at
204 different DC electrical field (n=4). **i**, Electroporation under condition: voltage 60 V;
205 pulse duration 100 μs; 5 pulses; pulse interval 1 s. Upper: HUVECs; middle: HAFs;
206 lower: SMCs. Blue represents cell nucleus, stained by DAPI; red represents cell
207 skeleton, stained by Rhodamine Phalloidin; green represents GFP; black represents
208 that cells were on the top of non-transparent MPC-PLC circuit, bright field. Scale bar,
209 20 μm.
210
211 ***In vitro* electroporation**
212 To further prove the functionality of the electronic blood vessel, we designed a comb-
213 like circuit pattern for electroporation (**Supplementary Fig. 1**). We connected the
214 cell-laden electronic blood vessel with an electroporator (BTX, CM630, US) to
215 generate DC pulses (**Fig. 3c**) and achieved the delivery of the green fluorescent
216 protein (GFP) DNA plasmid. To optimize the performance of the electronic blood
217 vessel, we found two major parameters determining the efficacy of electroporation,
218 including voltage and pulse duration. To realize the optimal efficacy, we exerted a

219 square wave with the voltage of 60 V, pulse duration of 100 μs, and pulse interval of 1
220 s for 5 times. We delivered GFP DNA plasmid into three kinds of blood vessel cells
221 and the GFP DNA realized expression with more than 95% of cells showing green
222 fluorescence (**Fig. 3i**). These promising *in vitro* results encouraged us to carry out the
223 *in vivo* tests of the electronic blood vessel.
224
225 **Mechanical properties of the electronic blood vessel**
226 To find out whether the electronic blood vessel is suitable for *in vivo* implantation, we
227 measured the mechanical properties, including stress-strain curve, compliance, and
228 burst pressure, of the electronic blood vessel with a diameter of 2 mm prior to
229 implantation (**Fig. 1m-r and Supplementary Fig. 3**). The elastic modulus of the
230 electronic blood vessel is about 130 MPa, the value is much higher than the native
231 carotid artery. The ultimate tensile strength of the electronic blood vessel is about 27
232 MPa, the value is also much higher than that of the native carotid artery. The initial
233 compliance of the electronic blood vessel (n= 5) is about 5% per 100 mmHg in the
234 range of 80-120 mmHg, the value is apparently below that of the native carotid artery
235 (n= 3). The burst pressure of the electronic blood vessel (n= 5) is about 2800 mmHg,
236 the value is similar to that of the native carotid artery (n= 3). The elongation at break
237 of the electronic blood vessel is about 650% (n= 5), which is the twice as the value of
238 native carotid artery (n= 3). The mechanical property of electronic blood vessel was
239 considered robust enough for implantation.
240

241 ***In vivo* implantation in rabbits and *in situ* monitoring**

242 To investigate the electronic blood vessel as a vascular implant, we chose the New
243 Zealand rabbit (age: 200-300 days, body weight: 3-4 kg) as the animal model and
244 replaced the native carotid artery with the electronic blood vessel (**Fig. 4a-c**). To
245 avoid possible immunological response of the host tissue, we used the acellular
246 electronic blood vessel in the preliminary *in vivo* study. We *in situ* monitored the
247 implanted electronic blood vessel by doppler ultrasound imaging (**Fig. 4d-i**) and the
248 arteriography (**Fig. 4j, k**). Doppler ultrasound imaging showed that the electronic
249 blood vessel allowed for good blood flow 3 months post-implantation (**Fig. 4d-g and**
250 **Supplementary Video 1**). The asymmetric velocity curve synchronized with the
251 ultrasonic pulses indicated that the signal is from the carotid artery rather than the
252 vein (**Fig. 4d**). The diameter of the electronic blood vessel remained at a relatively
253 constant value, about 2.3 mm, during the half month to three months post-
254 implantation (**Fig. 4g, h**). The mean velocity of the blood flow in different samples at
255 different time point was about 0.47 m s^{-1}, which was in the range of the normal value
256 (**Fig. 4i**). As the gold standard of the blood vessel patency, arteriography showed that
257 the electronic blood vessel matched with the native carotid artery very well and
258 allowed for excellent blood flow (**Fig. 4j, k, Supplementary Fig. 4, and**
259 **Supplementary Video 2**). There was no sign of narrowing. The electronic blood
260 vessel allows straightforward visualization under arteriography because the liquid
261 metal-based circuitry has sufficiently high contrast over host tissues (**Fig. 4j**). The red
262 frame outlined the electronic blood vessel with an alternate strip structure from the

263 MPC circuit. We explanted the electronic blood vessel three months post-implantation
264 for characterization. The lumen and the outer surfaces of the explanted electronic
265 blood vessel were smooth, covered by the remodeling tissues (**Fig. 4l, m**). The
266 diameter of the native blood vessel significantly reduced due to the lack of the blood
267 pressure, whereas the electronic blood vessel remained the same as before
268 (**Supplementary Fig. 5**).

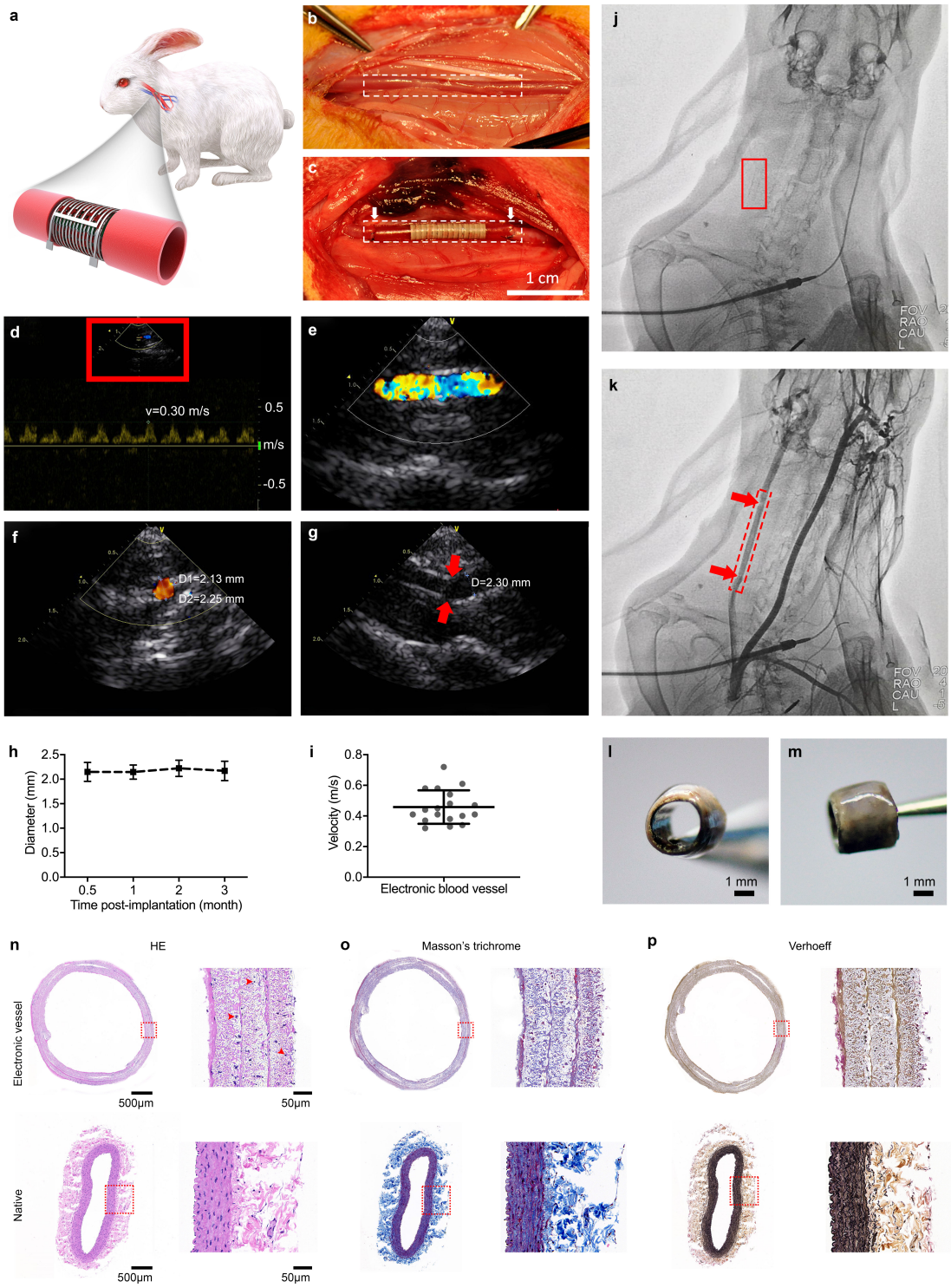

Fig. 4. ***In vivo and ex vivo*** **study of the electronic blood vessel. a**, Schematic of the electronic blood vessel in the carotid artery of the rabbit. **b, c**, An end-to-end anastomosis procedure of electronic blood vessel implantation on carotid arteries of rabbits (n=6). The dotted frames outline the margin of the native carotid artery and the

implanted electronic blood vessel. The white arrows indicate two ends of the electronic blood vessel. Scale bar, 1 cm. **d-g**, *In situ* monitoring of the electronic blood vessel by doppler ultrasound imaging 3 months post-implantation. Representative images from at least three different animals. **d, e**, The real-time blood flow at the operational site and the synchronized ultrasound pulses. The asymmetric velocity curve represents the signal is from carotid artery rather than vein. **e**, Zoom-in view of red box in (d). **f**, The cross view of the blood flow. **g**, The suture site (red arrows) connecting the native carotid artery and the electronic blood vessel. **h**, The diameter changes of the electronic blood vessel in different time post-implantation. **i**, The velocity of blood flow at the operational site (n=18, from different rabbits at different time points). **j, k**, *In situ* monitoring by arteriography 3 months post-implantation. **j**, Image before injecting the contrast media. Red box indicates the position of the implanted electronic blood vessel. **k**, Image after injecting the contrast media. Red box indicates the position of the implanted blood vessel. Red arrows indicate the suture sites connecting the native carotid artery and the electronic blood vessel. **l, m**, The cross-sectional view of the explanted electronic blood vessel after 3-month host remodeling. Scale bar, 1 mm. **n-p**, Hematoxylin/eosin (H&E) staining, Masson's trichrome staining, and Verhoeff's staining of the implanted electronic blood vessel 3 months post-implantation, setting native carotid artery as control. The right panel is the zoom-in view of the left panel. Scale bar (left), 500 μm. Scale bar (right), 50 μm.

296 ***Ex vivo* study**

297 To study the histological changes of the implanted electronic blood vessels, we
298 dissected all the implanted electronic blood vessels 3 months post-implantation and
299 performed histological staining of the electronic blood vessels, setting native carotid
300 blood vessel as a positive control. Hematoxylin/eosin (H&E) staining (**Fig. 4n**) of the
301 cross section of the electronic blood vessel is round-shaped, continuous, red, which is
302 similar to the native blood vessel. The three-layered MPC-PLC membrane merged
303 into one intact layer with secretion of substantial extracellular matrix between the
304 different layers of electronic blood vessel. We could clearly see dark blue nuclei in all
305 the layers, which indicated successful migration of host cells into the electronic blood
306 vessel. More importantly, a dense layer of cells with curved structure were formed in
307 the lumen of the electronic blood vessel which indicated the excellent endothelization
308 and thus ensured good blood flow. To further confirm the components in the
309 implanted electronic blood vessel, we performed Masson's trichrome (**Fig. 4o**) and
310 Verhoeff's staining (**Fig. 4p**). Masson's trichrome staining can stain and assess keratin
311 and muscle fibers (red) or collagen (blue) and Verhoeff's staining can stain and assess
312 the presence of elastin fibers. Masson's trichrome and Verhoeff's staining showed
313 well-distributed collagen and elastin fibers both inside the layers and between
314 different layers, indicating appropriate remodeling. Compared to the abundance level
315 of extracelluar matrix in the native blood vessel, the electronic blood vessel still
316 requires more time for material degradation and tissue remodeling. We also tested its
317 conductivity and the circuit in the electronic blood vessel was still conductive. These

results indicated that the electronic blood vessel was still functioning with the presence of conductive materials and host remodeling 3 months post-implantation.

To investigate the influence of the electronic blood vessel on the host, we performed the cross section and histological staining of the major organs, including heart, liver, spleen, lung, and kidney, together with the dissection of the implanted electronic blood vessel 3 months post-implantation. The H&E staining and Masson's Chrome staining showed that there was no significant pathological changes or inflammatory responses in these organs (**Supplementary Fig. 6**). To evaluate whether there were chronic inflammation or infection, we conducted the ELISA assay of three important proteins in the blood, including the interleukin-6 (IL-6), procalcitonin (PCT), and C-reactive protein (CRP) (**Supplementary Fig. 7**). The concentrations of IL-6 and PCT were not higher than the normal value of healthy rabbits (red dotted lines). The concentration of CRP was higher than the normal value of healthy rabbits (red dotted line). All three indexes decreased over time, a tendency that was expected. The results showed that most of the indexes were in the normal range and there were no significant pathological changes or inflammatory responses. These results confirmed that as an implant for vascular system, the electronic blood vessel had no significant detriment to the host.

Discussion

None of the existing small-diameter TEBVs has met the demands in treating cardiovascular diseases. Conventional TEBVs can be greatly improved to provide next-generation treatment by integrating with flexible bioelectronics. In this work, we report an electronic blood vessel with excellent biocompatibility, flexibility, mechanical strength, and degradability by combining the MPC with a US FDA-approved biodegradable polymer. As a proof of concept, we verified that the electronic blood vessel can accelerate the HUVEC proliferation and migration by electrical stimulation, thus facilitating the endothelization process, which is important to an engineered vascular conduit in preventing early thrombosis. Because most TEBVs occluded with 2 weeks post-implantation, our electronic blood vessel, with a patency of at least 12 weeks, is of great promise for clinical application. We also showcased that it could be used to perform *in situ* gene delivery via electroporation, which laid a foundation for future design and optimization such that we can carry out further gene therapies targeting different pathological problems after implantation. The electronic blood vessel has a high level of safety. The liquid metal[16,27] has been proven to be highly biocompatible and the PLC has been approved by the US FDA for implants[28]. We validated its biosafety in the vascular system by a 3-month implantation in a rabbit carotid artery model. Both the *in situ* monitoring, including doppler ultrasound imaging and arteriography, and *ex vivo* study demonstrated that it was safe as an electronic implant in the vascular system and at the body level.

As a vascular substitute, it breaks through the limitations of the existing vascular

scaffold by endowing the electrical function to conventional biodegradable TEBV and provides us a new platform for tackling the problems threatening the small-diameter blood vessel. By integrating with other electronic devices, the electronic blood vessel can provide various treatments, such as electrical stimulation, electroporation, electrically controlled drug release, and so forth. When combining with emerging technologies such as artificial intelligence, it can greatly boost future personalized medicine by bridging the vascular tissue-machine interface and empowering the health data collection and storage, such as blood velocity, blood pressure, and blood glucose level. In the future, optimizing its function and creating a multifunctional electronic blood vessel can greatly benefit human cardiovascular health.

370 **References**

371 1. WHO | World Health Statistics 2019: Monitoring health for the SDGs. *World*
372 *Heal. Organ.* (2019).

373 2. Seifu, D. G., Purnama, A., Mequanint, K. & Mantovani, D. Small-diameter
374 vascular tissue engineering. *Nat. Rev. Cardiol.* **10**, 410–421 (2013).

375 3. Quint, C. *et al.* Decellularized tissue-engineered blood vessel as an arterial
376 conduit. *Proc. Natl. Acad. Sci.* **108**, 9214–9219 (2011).

377 4. Dahl, S. L. M. *et al.* Readily available tissue-engineered vascular grafts. *Sci.*
378 *Transl. Med.* **3**, 68ra9 (2011).

379 5. Lawson, J. H. *et al.* Bioengineered human acellular vessels for dialysis access
380 in patients with end-stage renal disease: two phase 2 single-arm trials. *Lancet*
381 **387**, 2026–2034 (2016).

382 6. Zhu, M. *et al.* In vivo engineered extracellular matrix scaffolds with instructive
383 niches for oriented tissue regeneration. *Nat. Commun.* **10**, 4620 (2019).

384 7. Kirkton, R. D. *et al.* Bioengineered human acellular vessels recellularize and
385 evolve into living blood vessels after human implantation. *Sci. Transl. Med.* **11**,
386 1–12 (2019).

387 8. L'Heureux, N. *et al.* Human tissue-engineered blood vessels for adult arterial
388 revascularization. *Nat. Med.* **12**, 361–5 (2006).

389 9. L'Heureux, N., McAllister, T. N. & de la Fuente, L. M. Tissue-engineered
390 blood vessel for adult arterial revascularization. *N. Engl. J. Med.* **357**, 1451–
391 1453 (2007).

392 10. L'Heureux, N. *et al.* Technology insight: the evolution of tissue-engineered
393 vascular grafts - from research to clinical practice. *Nat. Clin. Pract.*
394 *Cardiovasc. Med.* **4**, 389–395 (2007).
395 11. Peck, M., Dusserre, N., McAllister, T. N. & L'Heureux, N. Tissue engineering
396 by self-assembly. *Mater. Today* **14**, 218–224 (2011).
397 12. Wu, W., Allen, R. A. & Wang, Y. Fast-degrading elastomer enables rapid
398 remodeling of a cell-free synthetic graft into a neoartery. *Nat. Med.* **18**, 1148–
399 1153 (2012).
400 13. Cheng, S. *et al.* Self-Adjusting, polymeric multilayered roll that can keep the
401 shapes of the blood vessel scaffolds during biodegradation. *Adv. Mater.* **29**,
402 (2017).
403 14. Akentjew, T. L. *et al.* Rapid fabrication of reinforced and cell-laden vascular
404 grafts structurally inspired by human coronary arteries. *Nat. Commun.* **10**, 1–15
405 (2019).
406 15. Hoenig, M. R., Campbell, G. R., Rolfe, B. E. & Campbell, J. H. Tissue-
407 engineered blood vessels: alternative to autologous grafts? *Arterioscler.*
408 *Thromb. Vasc. Biol.* **25**, 1128–1134 (2005).
409 16. Yan, J., Lu, Y., Chen, G., Yang, M. & Gu, Z. Advances in liquid metals for
410 biomedical applications. *Chem. Soc. Rev.* **47**, 2518–2533 (2018).
411 17. Choi, S., Han, S. I., Kim, D., Hyeon, T. & Kim, D. H. High-performance
412 stretchable conductive nanocomposites: Materials, processes, and device
413 applications. *Chem. Soc. Rev.* **48**, 1566–1595 (2019).

414 18. Son, D. *et al.* Bioresorbable electronic stent integrated with therapeutic
415 nanoparticles for endovascular diseases. *ACS Nano* **9**, 5937–5946 (2015).
416 19. Du, Z. J., Bi, G. Q. & Cui, X. T. Electrically controlled neurochemical release
417 from dual-layer conducting polymer films for precise modulation of neural
418 network activity in rat barrel cortex. *Adv. Funct. Mater.* **28**, 1–12 (2018).
419 20. Gong, P. *et al.* A strategy for the construction of controlled, three-dimensional,
420 multilayered, tissue-like structures. *Adv. Funct. Mater.* **23**, 42–46 (2013).
421 21. Jin, Y. *et al.* Stress-induced self-assembly of complex three dimensional
422 structures by elastic membranes. *Small* **9**, 2410–4 (2013).
423 22. Yuan, B. *et al.* A strategy for depositing different types of cells in three
424 dimensions to mimic tubular structures in tissues. *Adv. Mater.* **24**, 890–896
425 (2012).
426 23. Wang, N. *et al.* A strategy for rapid and facile fabrication of controlled, layered
427 blood vessel-like structures. *RSC Adv.* **6**, 55054–55063 (2016).
428 24. Tang, L., Mou, L., Zhang, W. & Jiang, X. Large-scale fabrication of highly
429 elastic conductors on a broad range of surfaces. *ACS Appl. Mater. Interfaces*
430 **11**, 7138–7147 (2019).
431 25. Tang, L. *et al.* Printable metal-polymer conductors for highly stretchable bio-
432 devices. *iScience* **4**, 302–311 (2018).
433 26. Bai, H., McCaig, C. D., Forrester, J. V. & Zhao, M. DC electric fields induce
434 distinct preangiogenic responses in microvascular and macrovascular cells.
435 *Arterioscler. Thromb. Vasc. Biol.* **24**, 1234–1239 (2004).

436 27. Lu, Y. *et al.* Transformable liquid-metal nanomedicine. *Nat. Commun.* **6**,
437 10066 (2015).
438 28. Kenar, H. *et al.* Microfibrous scaffolds from poly(L-lactide-co-ε-caprolactone)
439 blended with xeno-free collagen/hyaluronic acid for improvement of
440 vascularization in tissue engineering applications. *Mater. Sci. Eng. C* **97**, 31–44
441 (2019).
442

443 **Data availability**

444 All data are available from the corresponding authors upon reasonable request.

445 **Acknowledgement**

446 This study was supported by the National Key R&D Program of China
447 (2018YFA0902600, 2017YFA0205901), the National Natural Science Foundation of
448 China (21535001, 81730051, 21761142006, 51973045), the Chinese Academy of
449 Sciences (QYZDJ-SSW-SLH039, 121D11KYSB20170026, XDA16020902),
450 Shenzhen Bay Laboratory (SZBL2019062801004), the Tencent Foundation through
451 the XPLORER PRIZE, Beijing Science and Technology Plan Project
452 (Z191100007619053), Postgraduate Innovation Foundation of Peking Union Medical
453 College (2019-1002-28) and Teaching Reform Foundation of Postgraduate Education
454 in Peking Union Medical College (10023201900202). We thank Dr. Zewen Wei and
455 Dr. Deyao Zhao for discussions on the electroporation experiment. We thank Mrs.
456 Barbara Althaus at EPFL for her advice in writing the manuscript.
457

Author Contributions

X. J. and S. C. conceived the idea. S. C. designed the experiments, fabricated the blood vessel, conducted the characterization, *in vitro* tests, mechanical tests, *in vivo* tests and *ex vivo* tests, analyzed the data, and wrote the manuscript. C. H. prepared the liquid metal particles and fabricated the blood vessel, performed *in vitro* tests, electrical stimulation study, mechanical tests, and *in vivo* tests. L. D. performed the *in vivo* and *ex vivo* tests. S. C., C. H., and L. D. contributed equally to this work. L. T. assisted with the preparation of the liquid metal particles, MPC-PLC membrane and the electroporation experiments. L. J. and Y. Z. performed the implantation of the electronic blood vessel, doppler ultrasound imaging and arteriography. L. M. conducted the ELISA assay. J. Q. and R. D. assisted the TEM characterization. W. Z. gave inputs on the *in vitro* tests and *ex vivo* tests. Y. Z. supervised the *in vivo* and *ex vivo* study. X. J. supervised the project, and revised the manuscript. All the authors took part in the discussion and writing.

Competing financial interests

S. C. and X. J. declare financial interest in form of a patent application. Other authors declare no competing financial interests.

Additional Information

Supplementary Information is available for this paper.

Correspondence and requests for materials should be addressed to: S. C. or X. J.